THE JOURNAL OF PHYSICAL CHEMISTRY A

Article

pubs.acs.org/JPCA

Reactivity and Selectivity of Boron-Substituted Alkenes in the Diels–Alder Reaction with Cyclopentadiene. A Study of the Electron Charge Density and Its Laplacian

Margarita M. Vallejos,*[,†] Nicolás Grimblat, and Silvina C. Pellegrinet*

Instituto de Química Rosario (CONICET), Facultad de Ciencias Bioquímicas y Farmacéuticas, Universidad Nacional de Rosario, Suipacha 531, Rosario 2000, Argentina

Supporting Information

ABSTRACT: The effect of the nature of the boron moiety upon the reactivity and the selectivity of a variety of vinylboron dienophiles (**1**–**12**) in the Diels–Alder (DA) reaction was investigated using density functional theory and the quantum theory of atoms in molecules. The calculated reactivity of the dienophiles decreases in the order vinylborane (**1**) > dihalovinylboranes (**2**–**4**) > dialkylvinylboranes (**5**–**7**) ≈ vinyl boronic acid (**8**) > vinylboronates (**9**, **10**) > vinyl MIDA boronate (**11**) ≈ vinyltrifluoroborate (**12**). The DA reactions of **1**–**7** were slightly *endo*-selective due to the stronger C_6–B secondary orbital interaction in the *endo* transition structures (TSs) evaluated by the C_6|B delocalization index. In the TSs of **5** and **7**, a combination of electronic and steric factors reduce the *endo* selectivity. The moderate *exo* selectivity calculated for the DA reactions of boronates **8**–**11** was attributed mainly to the hydrogen bond between the oxygen atom of boronate moieties and one of the acidic hydrogens of the methylene of cyclopentadiene in the *exo* TSs, which also reduces the ability of the oxygen lone pairs to donate electron density into the vacant boron orbital. Interestingly, the cooperative effect between the two hydrogen bonds in the *exo* TS of the DA reaction of vinyltrifluoroborate (**12**) determines the almost exclusive *exo* selectivity predicted for this DA reaction. We propose that the relative reactivities of the dienophiles can be estimated by the charge density (ρ_r) and its Laplacian ($\nabla^2\rho_r$) at the (3,+1) critical point in the topology of $\nabla^2\rho_r$, evaluated at the reactant molecules in the ground state. The profiles of the several topological parameters along the reaction are affected by the nature of the substituents attached to the boron atom and by the mode of addition (*endo* and *exo*) in the DA reactions.

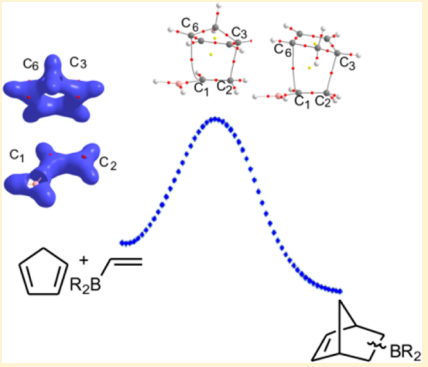

INTRODUCTION

Many synthetic routes toward the construction of the six-membered rings are possible through Diels–Alder (DA) reactions, which can involve a large variety of dienes and dienophiles.[1,2] By varying the nature of the reactants, it is possible to control the rate and selectivity of the DA reaction.[3] Boron-activated dienophiles have shown great versatility as building blocks in several DA reactions.[4,5] The substituent attached to the boron atom in the dienophiles greatly affects the outcome of the DA reactions. For example, the DA reactions of cyclopentadiene and vinylboranes such as dimethylvinylborane[6] and dichlorovinylborane[7,8] occur at a lower temperature than those for vinylboronic esters such as dibutylvinylboronate[9,10] and pinacol vinylboronate[11] and exhibit higher *endo* selectivities (Scheme 1).

Thus, alkenylboronic esters are less activated dienophiles than the corresponding dialkylvinylboranes and dihalovinylboranes, and the reactions require elevated temperatures and lead to cycloadducts with low *endo*/*exo* stereoselectivities. However, vinylboronates are more stable and easy to handle, whereas alkenylboranes often have to be prepared in situ and the cycloadducts derivatized. To explain the high reactivity and stereoselectivity of dialkylvinylboranes, Singleton[12] performed ab initio calculations and proposed the presence of an important nonclassical [4 + 3] C–B interaction in the *endo* transition structures (TSs) of the DA reactions of vinylborane and dimethylvinylborane. Later, Goodman et al.[13] showed that for the DA reactions of vinylborane with *trans*-piperylene and isoprene, the *endo* TSs have strong [4 + 3] character, although these led to the [4 + 2] cycloadducts, whereas in the *endo* TSs for reactions with dimethylvinylborane, the C–B interactions are weaker, adopting classical [4 + 2] character due to the greater size of the alkyl groups attached to the boron atom. Further computational studies on the DA reactions of several dienes with boron-substituted dienophiles also demonstrated that the [4 + 3] C–B secondary interactions get weaker as the electron-attracting character of the substituent attached to boron decreases, and the selectivities are governed by electronic and/or steric effects.[14,15]

The quantum theory of atoms in molecules (QTAIM), which is based on quantum mechanics and physical observables, is a key tool for the analysis of the electron charge density

Received: May 20, 2014
Revised: June 30, 2014
Published: July 1, 2014

Scheme 1

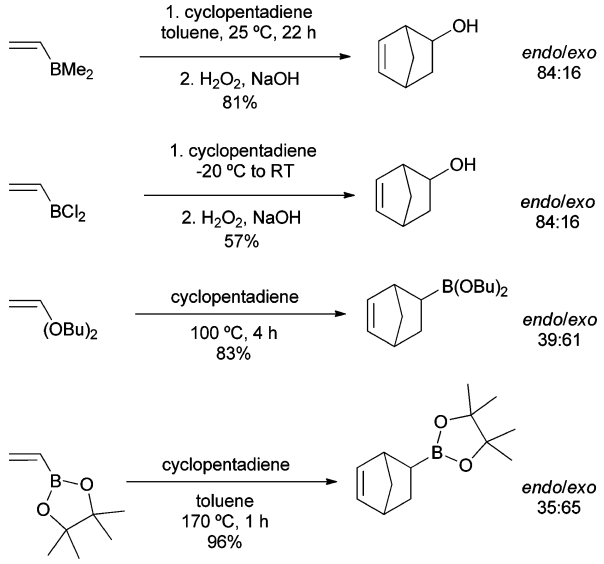

distribution.[16,17] Through this approach, it is possible to understand the electronic structure of molecules and their resulting chemical reactivity and also the nature and properties of chemical bonds.[18,19] In addition, the QTAIM topological analysis of the electron charge density and its Laplacian along the reaction path connecting the stationary points has been successfully applied to rationalize the mechanism of chemical reactions such as the dimerization of cyclopentadiene,[20] the Cope rearrangement of 1,5-hexadiene,[21] pericyclic and pseudopericyclic reactions,[22−27] among others.[28−30] Recently, we carried out a detailed QTAIM topological analysis along the course of the DA reactions of isoprene with unsaturated organoboron dienophiles, finding that the evolution of the [4 + 3] to the [4 + 2] structure observed in the *endo* pathway of the DA reaction with vinylborane occurs through a conflict mechanism in which the C_1 and B atoms of the dienophile compete to become attached to the C_6 atom of the diene.[31] The C_6−B secondary orbital interaction, present from early steps of the reaction until beyond the TSs, facilitates the formation of the new σ-bonds and is responsible for the higher charge concentration between the diene and the dienophile, which appears to account for the greater stabilization of the [4 + 3] TS.

In this work, we have performed a study within the QTAIM framework on the DA reactions of cyclopentadiene with boron-activated dienophiles **1**−**12** in order to gain a deeper insight into the effect of the nature of the boron moiety upon the distribution of the electron charge density in such a reaction (Scheme 2). Vinyl *N*-methyliminodiacetic acid (MIDA) boronate (**11**) and vinyltrifluoroborate (**12**) were selected because these tetracoordinated organoboron species have emerged as more convenient, economical, and versatile reagents for modern organic synthesis.[32−37] The forming bonds and the secondary orbital interactions between the diene and the dienophiles in the TSs were characterized by means of the QTAIM approach. We have also evaluated some topological parameters within the topology of the electron charge density and its Laplacian as potential indicators of reactivity of the dienophile and selectivity of the DA reactions.

Scheme 2

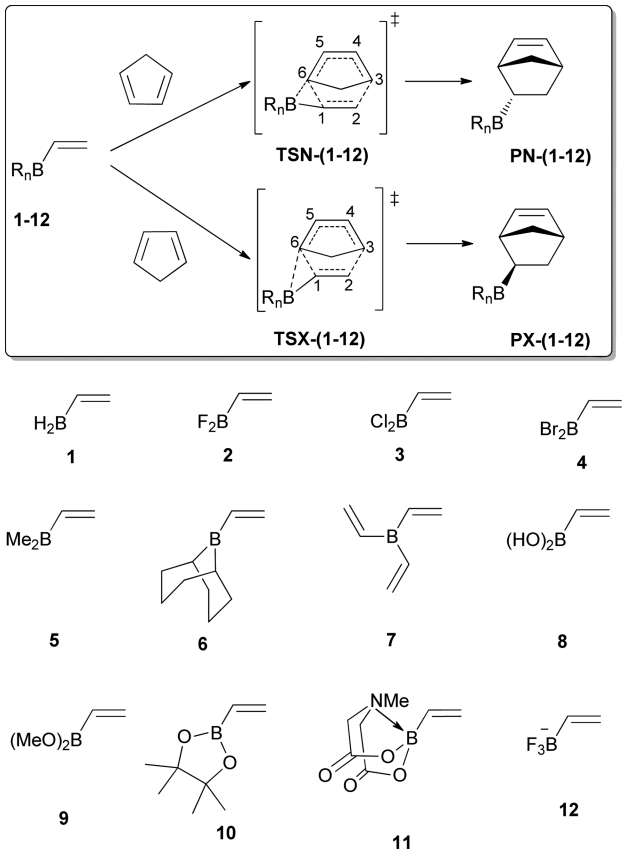

METHODOLOGY

The geometries of the reactants, the TSs, and the products were optimized without any constraints using DFT methods with the Becke3 Lee−Yang−Parr (B3LYP)[38,39] functional together with the 6-311++G(d,p) basis set. Frequency calculations were performed to verify the nature of the stationary points; TSs had one imaginary frequency, and the reactants and the cycloadducts had no imaginary frequencies. Zero-point vibrational energies (ZPVEs) were computed with the B3LYP/6-311++G(d,p) method and were not scaled. The intrinsic reaction coordinate (IRC) paths were traced in order to verify the connectivity of each TS with reactants and products using a step size of 0.10 Bohr. All calculations were carried out with the Gaussian 09 suite of programs.[40]

In accord with the QTAIM theory, a bond between two atoms is characterized by a line of maximum electron density, the bond path, that connects the respective nuclei and intersects the zero-flux surface of the electron density gradient field ($\nabla\rho_r$) at a topological (3, −1) critical point, called the bond critical point (bcp). Within this approach, different topological properties evaluated at the bcp are used to characterize the bonding interaction (calculated properties at the bcp in ρ_r topology are labeled with the subscript "b"): (1) the charge density, ρ_b, as a measure of accumulation of charge between the bonded nuclei, which reflects the bond strength; (2) the Laplacian of electron charge density, $\nabla^2\rho_b$, that provides information about the local charge concentration ($\nabla^2\rho_b < 0$) or depletion ($\nabla^2\rho_b > 0$);[16,17] and (3) the ellipticity, defined as $\varepsilon = (\lambda_1/\lambda_2) - 1$ (where λ_1 and λ_2 are the curvatures of the density at the bcp perpendicular to the bond path), which gives information about the charge distribution around

dx.doi.org/10.1021/jp504972r | J. Phys. Chem. A 2014, 118, 5559−5570

Table 1. Bond Distances (R), Gibbs Activation Energies ($\Delta G^{\#}$), Selectivities, and Charge Transfer (CT) from the Diene to the Dienophiles for the DA Reactions of 1−12 Dienophiles with Cyclopentadiene

	R (Å)					
TS	C_1-C_6	C_2-C_3	C_6-B	$\Delta G^{\#}$ (kcal mol^{-1})	*endo*/*exo* selectivity[a,b]	CT (e)[c]
TSN-1	2.527	2.032	2.460	30.15	58:42	0.154
TSX-1	2.580	2.043	2.694	30.35		0.153
TSN-2	2.493	2.020	2.899	32.58	55:45	0.153
TSX-2	2.498	2.037	2.905	32.71		0.151
TSN-3	2.599	1.996	3.022	30.99	61:39	0.192
TSX-3	2.605	2.013	3.039	31.26	(84:16)[7]	0.186
TSN-4	2.642	1.988	3.079	30.55	65:35	0.207
TSX-4	2.639	2.009	3.084	30.91		0.199
TSN-5	2.492	2.036	2.883	35.31	65:35	0.114
TSX-5	2.500	2.049	2.907	35.67	(84:16)[6]	0.111
TSN-6	2.509	2.031	2.991	35.86	41:59	0.113
TSX-6	2.515	2.045	2.973	35.63	(67:33)[45]	0.111
TSN-7	2.532	2.016	2.963	35.54	52:48	0.131
TSX-7	2.558	2.027	2.993	35.58	(78.22)[46]	0.128
TSN-8	2.377	2.086	2.955	36.08	26:74	0.083
TSX-8	2.426	2.064	2.959	35.46		0.089
TSN-9	2.457	2.034	3.033	37.06	32:68	0.082
TSX-9	2.436	2.059	2.974	36.62	(39:61)[9]	0.079
TSN-10	2.410	2.061	3.014	37.17	23:77	0.080
TSX-10	2.406	2.079	2.951	36.45	(35:65)[11]	0.077
TSN-11	2.304	2.114	2.995	37.78	33:67	0.115
TSX-11	2.309	2.126	2.962	37.33		0.107
TSN-12	2.180	2.275	3.001	39.22	3:97	−0.090
TSX-12	2.187	2.269	2.956	37.09		−0.097

[a]Ratios were computed using Boltzmann factors based on $\Delta G^{\#}$. [b]Experimental selectivities are shown in parentheses. [c]CT values were computed as the addition of the individual QTAIM charges of all of the atoms in the cyclopentadiene moiety.

the bond path and can be employed to determine the π character of a bond and also its stability.[25] The relationship $|V_b|/G_b$ (wherein V_b and G_b are the local potential and kinetic energies, respectively) and the total energy density, H_b (defined as the sum of the V_b and G_b), are used to analyze the covalent character of the interactions.[41] Furthermore, the delocalization index (DI) indicates the extent of exchange of electrons between two atomic basins, and it can be calculated between two atoms bonded by a bond path or without having a bond path to analyze the different interactions present in the TSs.[42]

For the QTAIM topological analysis, total electron densities were calculated at the B3LYP/6-311++G(d,p) level of theory. The bond and atomic properties were calculated using the AIMALL program.[43] The accuracy of the integration over the atomic basin (Ω) was assessed by the magnitude of a function $L(\Omega)$, which is less than 10^{-5} au for H atoms and 10^{-4} au for other atoms, in all cases.[44]

RESULTS AND DISCUSSION

Energetic, Geometric, and Electron Charge Density Analysis of the TSs. The DA reactions of cyclopentadiene and dienophiles **3**, **5**, **6**, **7**, **9**, and **10** have been previously investigated at the B3LYP/6-31G(d) level of theory and using the FMO approach.[14,15] We have re-examined the geometric and energetic parameters using the B3LYP/6-311++G(d,p) method. Overall, our results agreed with those reported before.

Bond distances and Gibbs activation energies ($\Delta G^{\#}$) for the DA reactions under study are presented in Table 1. The molecular graphs of the TSs for the *endo* and *exo* modes of addition between cyclopentadiene and selected dienophiles are shown in Figure 1 (the molecular graphs for remaining dienophiles are displayed in the Supporting Information). The topological properties evaluated at the forming bond bcps are listed in Table 2, which also includes the DIs.

The DA reactions of vinylborane **1** and dihalovinylboranes **2**−**4** presented the lowest activation energies (30.1−32.6 kcal mol^{-1}), which increased for dialkylvinylboranes **5**−**7** and the boronic acid derivative **8** (35.1−35.6 kcal mol^{-1}) and vinylboronates **9** and **10** (∼36.5 kcal mol^{-1}). The activation energies for the reactions of the tetracoordinated boron dienophiles **11** and **12** have the highest activation energies (∼37 kcal mol^{-1}). The lower reactivity of dienophiles **8**−**12** may be related to the conjugation between the lone pairs on the oxygen atoms and the vacant orbital of boron. In the tetracoordinated boron compounds (**11** and **12**), these latter orbitals are highly involved in the dative B−N bond of **11** and in the strong B−F bonds of **12**.

The calculated $\Delta G^{\#}$ values indicate that for the reactions of **1**−**5** and **7**, *endo* pathways are preferred, while for the reactions with the dienophiles **6** and **8**−**12**, the formation of the *exo* cycloadducts is more favorable. Interestingly, for the reaction of vinyltrifluoroborate (**12**), an excellent *exo* selectivity was computed (*endo*/*exo* 3:97), suggesting that the *exo* product (**PX-12**) would be obtained almost exclusively.

Overall, the calculated *endo*/*exo* selectivities reproduced the experimental ratios acceptably for the DA reactions of **3**, **5**, **9**, and **10**. For vinyl-9-BBN (**6**), the theoretical results predicted lower *endo*/*exo* selectivity, which probably is a consequence of a small difference in energy of the TSs corresponding to the *endo* and *exo* pathways, as was previously reported.[15]

The mechanisms of the DA reactions under study were predicted to be concerted because the TSs were connected

dx.doi.org/10.1021/jp504972r | J. Phys. Chem. A 2014, 118, 5559−5570

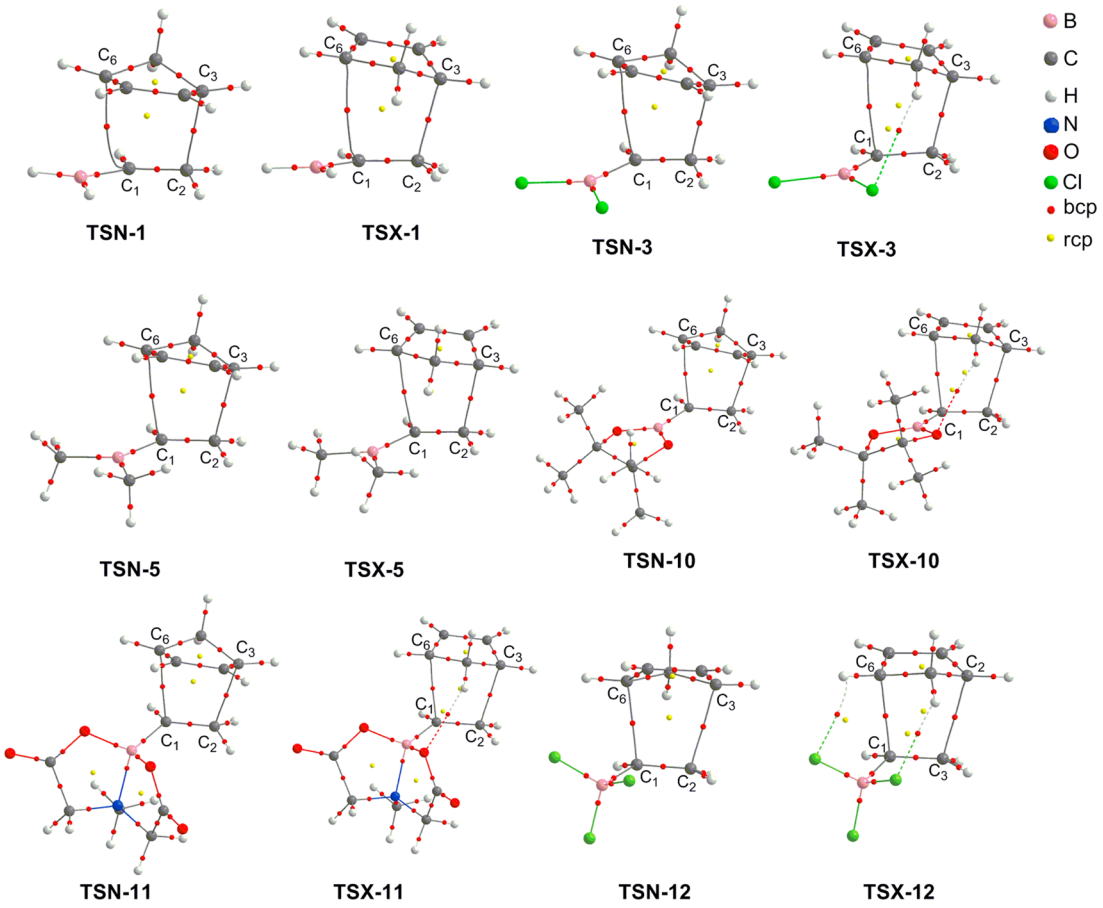

Figure 1. Molecular graphs of the TSs for the DA reactions of cyclopentadiene with dienophiles **1**, **3**, **5**, **10**, **11**, and **12**.

Table 2. Local Topological Properties for Selected bcps and DIs[a]

	ρ_b (au)		$\nabla^2\rho_b$ (au)		ε		$\lvert V_b\rvert/G_b$		H_b (au)		DI		
TS	C_1-C_6	C_2-C_3	C_1-C_6	C_2-C_3	C_1-C_6	C_2-C_3	C_1-C_6	C_2-C_3	C_1-C_6	C_2-C_3	C_1-C_6	C_2-C_3	C_6-B
TSN-1	0.0369	0.0794	0.0479	0.0130	1.2101	0.0130	1.1795	1.8799	−0.0026	−0.0239	0.286	0.489	0.099
TSX-1	0.0302	0.0769	0.0473	0.0192	0.4994	0.0382	1.0706	1.8233	−0.0009	−0.0224	0.268	0.471	0.057
TSN-2	0.0338	0.0814	0.0478	0.0127	0.3951	0.0497	1.1673	1.8879	−0.0024	−0.0251	0.300	0.489	0.028
TSX-2	0.0336	0.0784	0.0473	0.0176	0.1977	0.0557	1.1671	1.8409	−0.0024	−0.0233	0.298	0.474	0.024
TSN-3	0.0273	0.0850	0.0453	0.0070	0.4614	0.0484	1.0589	1.9404	−0.0007	−0.0274	0.247	0.502	0.035
TSX-3	0.0271	0.0818	0.0446	0.0122	0.2025	0.0519	1.0592	1.8925	−0.0007	−0.0254	0.248	0.487	0.031
TSN-4	0.0251	0.0862	0.0439	0.0050	0.4838	0.0486	1.0212	1.9576	−0.0002	−0.0282	0.228	0.506	0.037
TSX-4	0.0253	0.0823	0.0436	0.0113	0.2069	0.0516	1.0279	1.9010	−0.0003	−0.0257	0.233	0.489	0.033
TSN-5	0.0335	0.0788	0.0475	0.0161	0.4015	0.0417	1.1622	1.8536	−0.0023	−0.0235	0.295	0.482	0.036
TSX-5	0.0331	0.0766	0.0467	0.0199	0.1889	0.0484	1.1618	1.8171	−0.0023	−0.0222	0.295	0.470	0.030
TSN-6	0.0322	0.0795	0.0461	0.0158	0.3386	0.0441	1.1540	1.8583	−0.0021	−0.0239	0.290	0.482	0.032
TSX-6	0.0321	0.0770	0.0458	0.0198	0.1683	0.0495	1.1531	1.8192	−0.0021	−0.0225	0.289	0.469	0.028
TSN-7	0.0307	0.0821	0.0463	0.0116	0.3874	0.0430	1.1227	1.8978	−0.0016	−0.0254	0.271	0.493	0.032
TSX-7	0.0295	0.0799	0.0450	0.0157	0.1717	0.0467	1.1079	1.8603	−0.0014	−0.0241	0.266	0.481	0.027
TSN-8	0.0412	0.0720	0.0469	0.0257	0.2047	0.0577	1.3047	1.7519	−0.0051	−0.0195	0.337	0.453	0.017
TSX-8	0.0383	0.0746	0.0462	0.0227	0.1202	0.0600	1.2611	1.7870	−0.0041	−0.0210	0.325	0.460	0.016
TSN-9	0.0361	0.0792	0.0455	0.0169	0.2218	0.0508	1.2299	1.8483	−0.0034	−0.0237	0.314	0.479	0.017
TSX-9	0.0375	0.0752	0.0459	0.0220	0.1205	0.0577	1.2517	1.7952	−0.0039	−0.0214	0.321	0.463	0.016
TSN-10	0.0389	0.0753	0.0464	0.0219	0.2024	0.0549	1.2731	1.7963	−0.0044	−0.0214	0.327	0.464	0.017
TSX-10	0.0394	0.0725	0.0466	0.0256	0.1230	0.0616	1.2778	1.7560	−0.0045	−0.0198	0.328	0.451	0.016
TSN-11	0.0477	0.0685	0.0443	0.0298	0.1421	0.0684	1.4111	1.7021	−0.0077	−0.0175	0.359	0.439	0.010
TSX-11	0.0475	0.0667	0.0436	0.0316	0.1104	0.0774	1.4123	1.6776	−0.0076	−0.0166	0.360	0.431	0.009
TSN-12	0.0588	0.0508	0.0389	0.0426	0.0652	0.0756	1.5668	1.4583	−0.0127	−0.0090	0.393	0.369	0.005
TSX-12	0.0580	0.0511	0.0385	0.0430	0.0476	0.0860	1.5624	1.4597	−0.0124	−0.0091	0.393	0.367	0.005

[a]See the text and Figure 1 for an explanation of the symbols and identification of atoms.

dx.doi.org/10.1021/jp504972r | J. Phys. Chem. A 2014, 118, 5559−5570

directly to the reactants and the products. All TSs were asynchronous, the C_2-C_3 distances (1.98−2.13 Å) being shorter than the C_1-C_6 distances (2.31−2.64 Å), except for the TSs of vinyltrifluoroborate (**12**), in which $RC_2-C_3 > RC_1-C_6$.

In all of the TSs, two new bcps corresponding to the forming C_1-C_6 and C_2-C_3 σ-bonds and a ring critical point associated with the six-membered ring were found that agree with the characteristic topological pattern of the TSs with [4 + 2] character (Figure 1).[22−24] For the TSs of **1**−**11**, the values of ρ_b at the C_1-C_6 bcps (0.025−0.047 au) were lower than those at the C_2-C_3 bcps (0.067−0.086 au), and for the TSs of dienophile **12**, the ρ_b values at the C_1-C_6 bcps (0.025−0.047 au) were slightly higher than those at the C_2-C_3 bcps (0.067−0.086 au), in agreement with the bond formation distances. The difference of ρ_b at C_1-C_6 and C_2-C_3 bcps also reflects the asynchronicity of the TSs. In this sense, a good linear correlation was obtained between the ΔR and $\Delta\rho_b$ (R^2 = 0.95; see the Supporting Information). For all of the TSs, $\nabla^2\rho_b > 0$, $|V_b|/G_b > 1$, and $H_b < 0$ at the C_1-C_6 and C_2-C_3 bcps, indicating that the nature of the forming bonds is partially covalent.[41,47] For the TSs under study except for the ones corresponding to **12**, the ellipticity values at the C_2-C_3 bcps were lower than those at the C_1-C_6 bcps, which denotes that the distribution of the electron density around the interaction line C_2-C_3 is more symmetrical than that around the C_1-C_6 interaction, in accordance with the degree of formation of the σ-bonds.

In the *endo* TS of the reaction with vinylborane (**1**) (**TSN-1**), the C_6-B distance (2.460 Å) was shorter than the C_1-C_6 distance (2.527 Å), and the DI of C_1-C_6 had a considerable value (0.10), denoting that this TS had [4 + 2] character with a significant nonclassical C_6-B orbital secondary interaction. Previously, we found that the *endo* TSs of the DA reaction of vinylborane and isoprene have [4 + 3] character, characterized by two new bcps (C_2-C_3 bcp and C_6-B bcp) and a ring critical point corresponding to a seven-membered cyclic structure.[31] The C_6-B bcp was not found in **TSN-1**, but it exhibited a significant C_6-B interaction that might be responsible of its lower barrier energy. For the remaining TSs, C_6-B distances were longer than C_1-C_6 distances. As expected, the DIs of C_6-B were lower (0.04−0.01), in particular, for the TSs of reactions with dienophiles **8**−**12**, denoting a weak C_6-B secondary orbital interaction. For the reactions with dienophiles **2**−**7**, DI C_6-B values were higher in *endo* TSs, while for the reactions with dienophiles **8**−**12**, those values were of the same magnitude for both *endo* and *exo* TSs. The experimental *endo* selectivity of the DA reactions of cyclopentadiene with dienophiles **3**, **5**, and **6** was attributed to the C_6-B secondary orbital interaction in the *endo* TSs evaluated by the Wiberg bond indexes. Therefore, the lower *endo* selectivity calculated for the reaction of **6** might be related to the greater size of the substituent.[15]

Interestingly, in the *exo* TSs of the reactions with **2**−**4** and **7**−**12**, a hydrogen bond interaction was found with one of the acidic protons of the methylene of cyclopentadiene as the proton donor and an atom of the substituent attached to boron as the proton acceptor (Figure 1). In **TSX-12**, another hydrogen bond interaction between the C_6-H of cyclopentadiene and a fluorine atom was also localized. The interaction distances and topological properties of the hydrogen bonds are shown in Table 3. The hydrogen bond interactions were calculated to be weak hydrogen bonds because the H···X bond lengths lie between 2.31 and 2.82 Å.[48] In addition, the ρ_b at the H···X bcps were low (0.008−0.012 au), and the values of $\nabla^2\rho_b$ were positive within the range of 0.025−0.047 au. These values are within commonly accepted values for hydrogen bond interactions (for ρ_b from 0.002 to 0.040 au and for $\nabla^2\rho_b$ from 0.020 to 0.150 au)[49] and also indicated that the intermolecular interactions can be classified as "closed-shell" interactions. In addition, for the bcps corresponding to hydrogen bonds, $\nabla^2\rho_b > 0$ and $H_b > 0$, revealing that these interactions were mainly electrostatic in nature.[50]

Table 3. Bond Distances and Local Topological Properties for Hydrogen Bonds (H···X) in TSs[a]

TS	hydrogen bond	$R_{H\cdots X}$ (Å)	ρ_b (au)	$\nabla^2\rho_b$ (au)	$\lvert V_b\rvert/G_b$	H_b (au)
TSX-2	$H_a\cdots F$	2.446	0.0092	0.0351	−0.8407	0.0012
TSX-3	$H_a\cdots Cl$	2.726	0.0093	0.0305	−0.7575	0.0015
TSX-4	$H_a\cdots Br$	2.825	0.0095	0.0281	−0.7784	0.0013
TSX-7	$H_a\cdots C$	2.632	0.0084	0.0255	−0.7854	0.0011
TSX-8	$H_a\cdots O$	2.447	0.0103	0.0350	−0.8350	0.0012
TSX-9	$H_a\cdots O$	2.432	0.0109	0.0360	−0.8477	0.0012
TSX-10	$H_a\cdots O$	2.569	0.0085	0.0287	−0.8316	0.0010
TSX-11	$H_a\cdots O$	2.431	0.0104	0.0354	−0.8431	0.0012
TSX-12	$H_a\cdots F$	2.314	0.0120	0.0426	−0.8781	0.0012
	$H_6\cdots F$	2.370	0.0118	0.0473	−0.8516	0.0015

[a] H_a is one of the acidic protons of the methylene of cyclopentadiene.

Taking into account that hydrogen bonding involves a CT from the proton acceptor to the proton donor, this interaction can exert two different indirect electronic effects on the system, depending on the acceptor of the proton.[51] In the *exo* TSs of **2**−**4**, the hydrogen bond C−H···X (X = F, Cl or Br) could reduce the electron-withdrawing effect of the halogen atom, which is opposite of the stabilizing effect of this interaction. Thus, the slightly stronger C_6-B secondary interaction in *endo* TSs of the DA reactions of **2**−**4** could be an important factor in the selectivity of these reactions. The nonclassical hydrogen bond C−H···C in the *exo* TS of **7** is a weak interaction and does not play an important role in the stabilizations of this. In the case of the *exo* TSs of **8**−**11**, the hydrogen bond C−H···X (X = O) reduces the ability of the oxygen lone pairs to donate charge density into the vacant boron orbital. As both *endo* and *exo* TSs present similar C_6-B secondary orbital interactions, we infer that the effects of the hydrogen bond should play an important role in the *exo* selectivity of these reactions. In particular, the higher stability of the *exo* TS of the reaction with **12**, with similar C_6-B orbital secondary interactions for both TSs, may be explained by the cooperative effect of the two hydrogen bonds in the *exo* TS among the two fluorine atoms and the hydrogen atoms of cyclopentadiene.

On the other hand, the calculated CTs indicate that in the TSs, the flow of electron density is from the diene toward the dienophile (positive sign), except in the TSs of **12**, in which the flow is inverted (negative sign) (Table 1). In the TSs of dienophile **12**, the electron charge distribution is different from those in the other TSs, which may be related to the peculiar forming bonds. For the DA reactions, it has been proposed that an increase of the CT in the TSs is associated with a decrease of the energetic barrier.[52,53] Moreover, other studies indicated that for the same DA reactions, CT values did not correlate well with activation, and thus, care should be exercised when

dx.doi.org/10.1021/jp504972r | J. Phys. Chem. A 2014, 118, 5559−5570

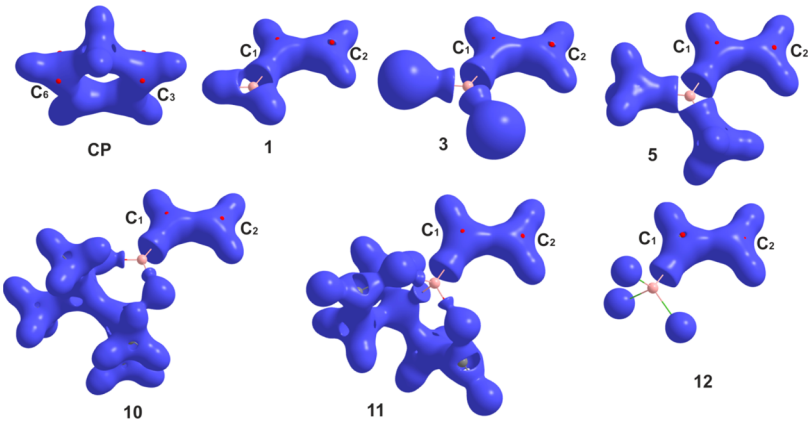

Figure 2. Envelops of the Laplacian of the electron density at L_r = 0.00 au for cyclopentadiene and selected dienophiles. The (3, +1) critical points of L_r for the atom participating in the forming bond of the DA reactions are denoted with red spheres.

estimating reactivity trends from CT. For the present investigation, acceptable linear correlation between the CTs and the activation energies (R^2 = 0.85) was obtained. The TSs of dienophiles **1** and **12** do not fit in this correlation due to a considerable secondary orbital[15,31,54] interaction found in **TSN-1** and the inverse flow of electron charge in the TSs of **12**.

Laplacian of the Electron Density in Isolated Reactant. The Laplacian of ρ_r provides an enhanced view of the local form of the electron density, and its topology can show in a molecular graph the localization of the preferential reactive sites for the nucleophiles and the electrophiles and has been used as an indicator to predict chemical reactivity.[31,55−57] For example, for the Michael addition, the relative reactivity of the activated double bond of a series of molecules (acrylic acid, methacrylic acid, acrylonitrile, and acrolein) toward a nucleophilic attack was predicted by the values of $\nabla^2\rho_r$ at the corresponding critical point and was in agreement with the experimental data.[58] Such analysis was carried out herein to predict the reactivities of boron-activated dienophiles in DA reactions using the isolated reagents. It is convenient to introduce the function $L_r = -1/4\nabla^2\rho_r$ because its density is locally concentrated or depleted.[55] The valence shell of an atom is divided into an inner region where $L_r > 0$ (called the valence shell charge concentration, VSCC) and an outer one where $L_r < 0$. The critical points in the distribution of the L_r function provide the precise localization of different reactivity zones. A (3, −3) critical point corresponds to a local maximum in L_r and indicates a local electron charge concentration ($L_r > 0$), while a (3, +3) critical point corresponds to a local minimum in L_r and indicates a local depletion of the electron charge ($L_r < 0$). Saddle points might be either (3, −1) or (3, +1) critical points. The envelops of the Laplacian of the charge density at L_r= 0.00 au for cyclopentadiene and selected dienophiles are displayed in Figure 2. Cyclopentadiene exhibits (3, +1) critical points of L_r on C_3 and C_6, and the dienophiles present (3, +1) critical points on C_1 and C_2 above and below the molecular plane. These critical points may be correlated with centers of interaction of the diene and dienophile in the DA reactions. In Table 4, the values of the ρ_r and L_r at the (3, +1) critical point of L_r are shown.

The (3, +1) critical points at C_3 and C_6 of cyclopentadiene were localized in a zone of charge concentration ($L_r > 0$), and the values of L_r at these critical points were more positive (0.0746 au) than those at critical points at C_1 and C_2 of the dienophiles. The (3, +1) critical points on C_2 for dienophiles **1**−**6** were found in a region of charge depletion ($L_r < 0$), while (3, +1) critical points at C_1 were placed in a region of charge concentration ($L_r > 0$). The regions of charge depletion on the carbon atoms have been associated with sites of nucleophilic attack in methanol and similar compounds.[58,59] Thus, C_2 is more susceptible to nucleophilic attack than C_1, and this finding may be related to the formation of the C_2−C_3 bond being more advanced than the C_1−C_6 bond. For dienophiles **7**−**11**, the (3, +1) critical points of both C_1 and C_2 were found in regions of charge concentration. However, ρ_r was smaller and L_r less positive at the (3, +1) critical points on the C_2 atom than those on C_1, predicting that for the DA reactions of cyclopentadiene with these dienophiles, the interaction between C_2 and C_3 would be more favorable than that between C_1 and C_6, which is in agreement with the bond distances and ρ_b evaluated at the corresponding bcps. In dienophile **12**, the (3, +1) critical points of L_r on C_1 were found in a region of charge depletion, and those on C_2 were placed in a region of charge concentration, indicating that the formation of C_1−C_6 would be more favorable, in accordance with the geometrical and topological data of their TSs. The greater the charge depletion, the more susceptible to nucleophilic attack the C_2. Interestingly, a good linear correlation between ρ_r and L_r at the (3, +1) critical points

Table 4. Properties of the Laplacian of the Charge Density at the (3, +1) Critical Points in the VSCC of the Reactants Evaluated on Selected Atoms along with the Electrophilicity Indices (ω)

reactants	ρ_r (au)		L_r (au)		ω (eV)
	C_3 and C_6		C_3 and C_6		
cyclopentadiene	0.1692		0.0746		1.12
	C_1	C_2	C_1	C_2	
1	0.1545	0.1450	0.0196	−0.0202	2.37
2	0.1605	0.1479	0.0383	−0.0121	2.06
3	0.1602	0.1469	0.0400	−0.0148	2.53
4	0.1601	0.1465	0.0406	−0.0155	2.68
5	0.1553	0.1500	0.0255	−0.0035	1.80
6	0.1551	0.1493	0.0220	−0.0057	1.80
7	0.1540	0.1517	0.0160	0.0024	2.37
8	0.1595	0.1518	0.0364	0.0026	1.46
9	0.1584	0.1525	0.0323	0.0054	1.37
10	0.1578	0.1535	0.0270	0.0087	1.33
11	0.1585	0.1555	0.0228	0.0124	1.40
12	0.1696	0.1466	−0.0137	0.0641	0.00

dx.doi.org/10.1021/jp504972r | J. Phys. Chem. A 2014, 118, 5559−5570

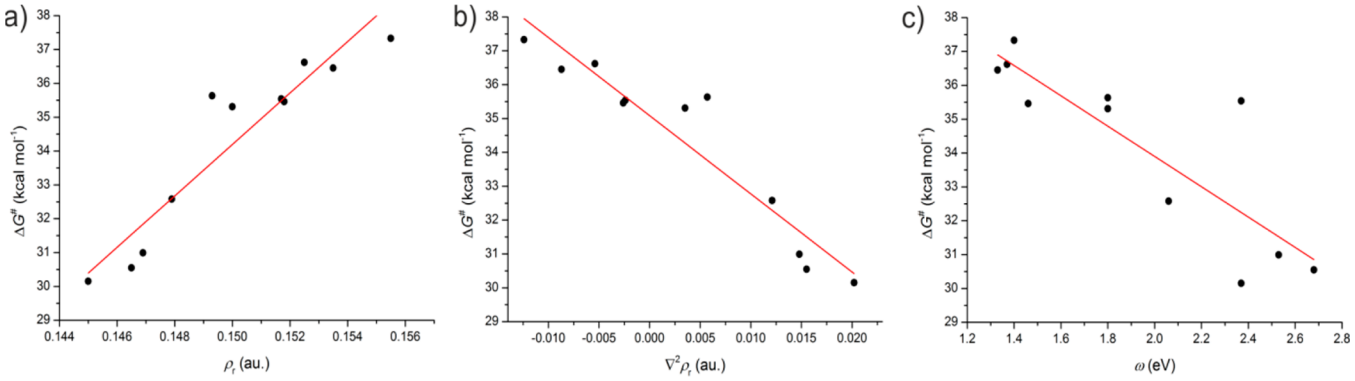

Figure 3. Activation free energy versus the values of (a) ρ_r, (b) $\nabla^2\rho_r$ at the (3, +1) critical points of the L_r corresponding to the C_2 atom, and (c) the electrophilicity index.

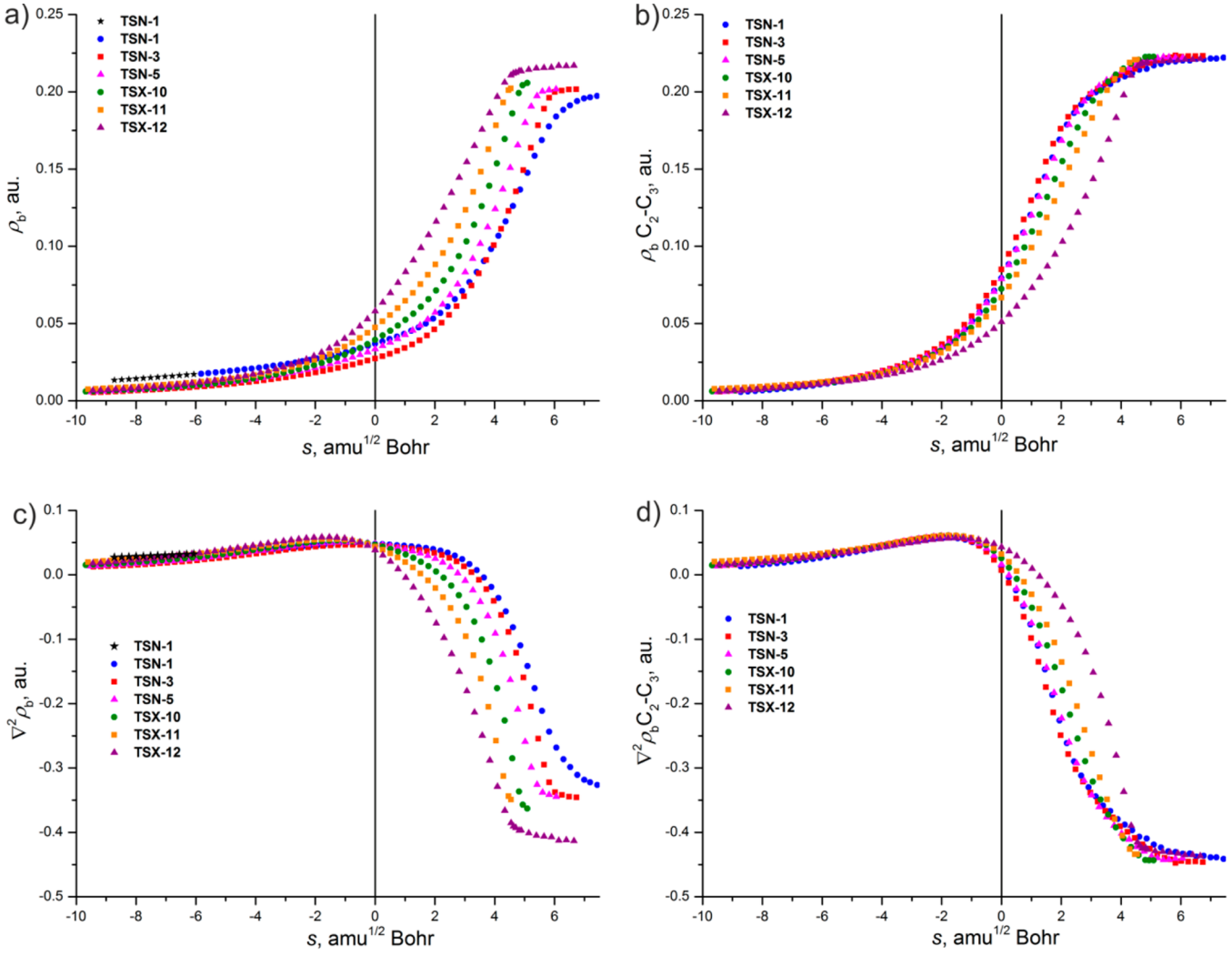

Figure 4. ρ_b and $\nabla^2\rho_b$ at the (a,c) C_1-C_6 bcp and (b,d) C_2-C_3 bcp along the IRC for selected channels of the DA reactions. Note that in (a) and (b), for the reaction associated with **TSN-1**, the points indicated with a black star correspond to the C_6-B bcp.

on C_2 and the activation free energy ($\Delta G^{\#}$) was obtained for dienophiles **1**−**11** (R^2 = 0.87 for both relationships; Figure 3). Vinyltrifluoroborate (**12**) did not fit into these correlations due to its anionic nature, which confers a particular feature on this dienophile.

The global electrophilic index (electrophilicity) of the reagents in their ground state has been used to estimate the activation barrier of the polar DA reaction.[52] Therefore, we performed an analysis of the electrophilicity of the reagents to correlate such results with those obtained with the Laplacian of the charge density analysis. The global electrophilicity indexes, ω, for the reagents are displayed in Table 4 (last column).[60] A linear correlation between the activation free energy and the ω index of the dienophiles under study, except dienophile **12**, was

dx.doi.org/10.1021/jp504972r | J. Phys. Chem. A 2014, 118, 5559−5570

also found, although the data did not fit as well as that with the other parameters (R^2 = 0.70).

According to these results, the Lapacian of the charge density analysis may be a useful tool not only to identify the reactive site in a dienophile but also to properly estimate the reactivity of neutral boron-activated dienophiles. It is worth mentioning that this conclusion is based on a real physical property of the system, the electron charge density that can be obtained by either experimental or computational methods.

Evolution of the Local Properties of ρ(r) and the Atomic Population along the Reaction Paths. Recent theoretical studies have shown that the analysis of the electron density along the reaction channel is a powerful tool to understand the mechanisms of DA reactions.[31] Such analysis was carried out to obtain more insight about the effect of the nature of the boron moiety on the distribution of the electron density in the course of these reactions. We analyzed the reactions of **1**, **3**, **5**, **10**, **11**, and **12** as models of different boron moieties. Overall, the trends of the ρ_b and $\nabla^2\rho_b$ at the bcps corresponding to the forming bonds (C_1-C_6 and C_2-C_3) along both *endo* and *exo* pathways were similar to only a slight difference in the magnitude (see the Supporting Information); thus, the changes in these topological properties are shown for the lowest-energy pathways of each reaction. The variations of ρ_b and $\nabla^2\rho_b$ at the C_1-C_6 and C_2-C_3 bcps along the IRC for selected reactions are displayed in Figure 4.

It is interesting to note that in the *endo* pathway of the reaction with **1**, the C_6-B bcp was found in early stages of the reaction (from ∼−9 to −6 amu$^{1/2}$ Bohr); then it disappeared, and suddenly, the C_1-C_6 bcp appeared. ρ_b at the C_6-B bcp had low values (from 0.0134 to 0.0172 au), and the values of $\nabla^2\rho_b$ were positive, denoting the weak nature of this interaction. This finding reflected that the *endo* pathway of the DA reaction with **1** evolves from a [4 + 3] to a [4 + 2] structure; thus, the system goes through a conflict point, in which the C_1 and B atoms compete to be the attractor of the charge density of the bond path that connects with C_6. Such particularity was observed for the *endo* pathway of the DA reaction of vinylborane with isoprene, but the conflict point that appeared after the TSs and the C_6-B interaction was stronger, with characteristics of a "shared shell" interaction being responsible for the low barrier energy of this reaction.[31]

As was noted in the analysis of the TSs, the formation of the C_2-C_3 bond was more advanced than that of the C_1-C_6 bond. When comparing the selected dienophiles, the increment of ρ_b and the change of sign of $\nabla^2\rho_b$ (from positive to negative) at the C_1-C_6 bcp occurred more rapidly in the order **1** < **3** < **5** < **10** < **11** < **12**, which indicates the strengthening of the C_1-C_6 interaction. The C_2-C_3 interaction becomes stronger in the reverse order. Furthermore, as C_2-C_3 formation is more advanced, the profiles of ρ_b and $\nabla^2\rho_b$ at C_2-C_3 bcp become more different to those evaluated at the C_1-C_6 bcp, and this explains why the reactions become more favorable energetically. Moreover, for the reaction with the highest energy barrier, that is, with **12**, the trajectories of both topological properties at the C_1-C_6 and C_2-C_3 bcps are very close.

The DI of C_6|B was evaluated along the selected reaction coordinates, considering the *endo* and *exo* pathways to evaluate the behavior of the C_6-B secondary interaction (Figure 5). The values of DI of C_6-B were low throughout the course of all reactions except for that of vinylborane (**1**). The DI of C_6|B reached maximum values after the TSs for the reactions with **1**, **3**, and **5** (0.11 for **TSN-1**, 0.08 for **TSX-1**, and ∼0.04 for

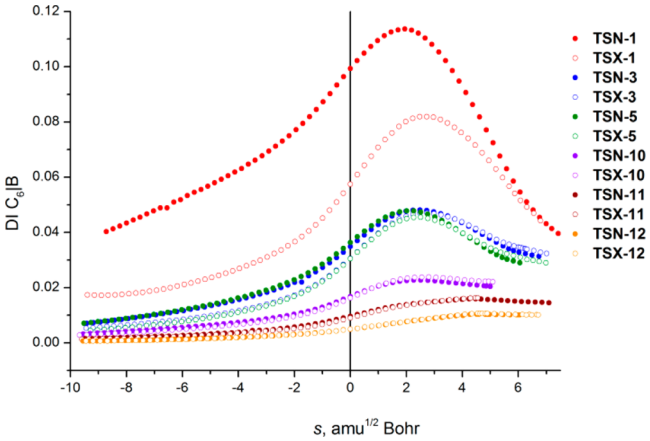

Figure 5. C_6|B DI along the IRC of selected DA reactions. The *endo* and *exo* channels are indicated with solid and open symbols, respectively.

reaction with **3** and **5**). For the reactions with **10**−**12**, the DI C_6-B values were <0.02 along the reaction coordinates. For the DA reaction of isoprene and vinylborane, the *meta* selectivity was attributed to the stronger C_6-B secondary orbital interaction in the *meta endo* pathway for which the values of the DI of C_6|B showed a bell-shaped profile, with a maximum value of 0.31.[31] Thus, the low *endo* selectivity calculated for the reaction with **1** (*endo*/*exo* 58:42) may be partially attributed to the same interaction. This interaction is weaker in the *exo* pathways for the reactions with **3** and **5**, which can also contribute to determine the *endo*/*exo* selectivities. The C_6-B secondary interaction becomes less important for the reactions with **10**−**12**. These results support the idea that the combination of electronic and steric effects is responsible for the observed selectivities of these reactions.

It has been previously demonstrated that the ellipticity profile evaluated at the bcp corresponding to a forming or breaking bond along the reaction coordinate constitutes a good indicator to distinguish pericyclic and pseudopericyclic reactions.[22−26] In addition, for the DA reactions of the isoprene and boron-substituted dienophiles, the ellipticity evaluated at the forming bond next to the boron atom was found to be a useful parameter to differentiate the pathways associated with [4 + 3] or [4 + 2] TSs and to distinguish between *endo* and *exo* modes of addition.[31] The ellipticity profiles evaluated at the C_1-C_6 bcps for both channels of selected dienophiles are shown in Figure 6.

For the reaction with dienophile **1**, the ellipticity profiles of the *endo* and *exo* pathways were very different. For the *endo* channel, the ellipticity increased up to a maximum of 1.21, which appeared at the TS; then it decreased to values close to zero. For the *exo* channel, the ellipticity decreased monotonically from 1.14 to values close to zero as the reaction proceeded, and no maximum was observed. The bell-shaped profile of ε observed for the pathway associated with **TSN-1** may be a consequence of the stronger C_6-B secondary orbital interaction. The reactions of dichlorovinylborane (**3**) and dimethylvinylborane (**5**) in the *endo* pathways showed relatively high ε values at the beginning of the reactions, with maximum values of 1.57 and 1.05, respectively, and then decreased progressively toward product formation. In the *exo* pathways, the ε decreased more abruptly as the reaction proceeded, showing a similar profile to the *exo* channel of the reaction with

dx.doi.org/10.1021/jp504972r | J. Phys. Chem. A 2014, 118, 5559−5570

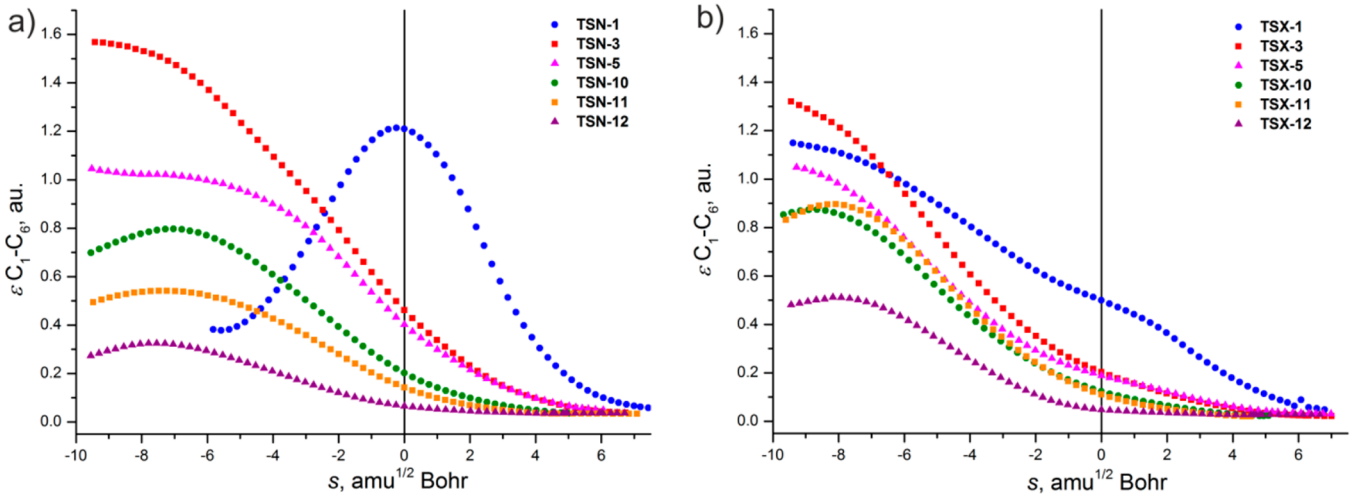

Figure 6. Ellipticity (ε) at the C_1–C_6 bcp along the IRC for the (a) *endo* and (b) *exo* pathways of the selected reactions.

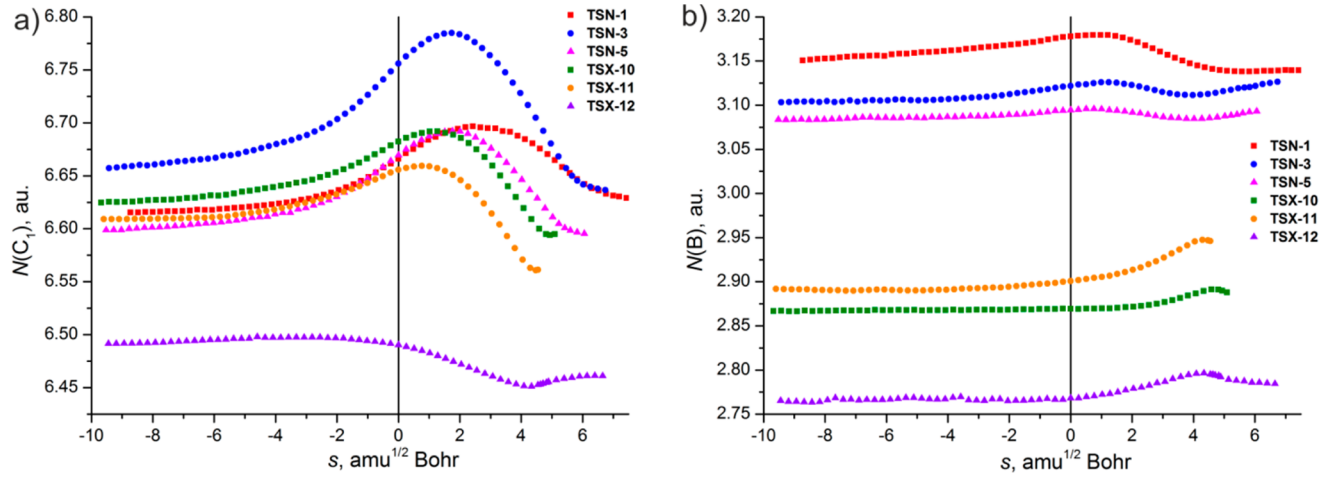

Figure 7. Electron population of the (a) C_1 and (b) B atoms along the IRC for the lowest pathways of the selected DA reactions.

1. In the case of the reactions with vinylboronates **10** and **11** and vinyltrifluoroborate (**12**), the changes of ε were less pronounced than those described above, indicating that the electron density undergoes smaller changes in the course of the reaction. In the first stages of the *exo* channels, the values of ε were higher than those of the *endo* counterparts, in particular for the reaction with **11**; then for both *endo* and *exo* pathways, the ε decayed, but in the latter, it was more abrupt. Both *endo* and *exo* pathways show a maximum of ε before the TS, being higher for the latter.

The ellipticity at the bcp provides a measure of the extent to which the electron density is asymmetrically distributed in perpendicular directions away from the bond axis.[61] Thus, these results show clearly that for the DA reactions with boranes **1**, **3**, and **5**, the changes of the electron density in the C_1–C_6 bonding region are more significant that for those with boronates **10** and **11** and trifluoroborate **12**. Furthermore, the changes of the electron density were more pronounced for the *endo* pathways of the reactions with **1**, **3**, and **5** and the *exo* pathway of the reaction with **10**–**12**, denoting that the electron distribution is strongly related to the stabilization of the system and therefore to the selectivities. Consequently, although the C_6–B interaction is weaker, the boron atom affects the surrounding distribution of the electron charge density to different extents, depending on the nature of the substituent attached to it and the mode of addition (*endo* or *exo*), which is reflected in the stabilization of the system and therefore in the selectivity of the reactions.

The atomic electron population $N(\Omega)$, defined by QTAIM as integrations of the electron density over the atomic basin (Ω), can be used to calculate the corresponding atomic net charge as $q(\Omega) = N(\Omega) - Z\Omega$ ($Z\Omega$ being the atomic number).[17,62−65] In general, similar trends of the electron populations of the C_1, C_2, C_3, C_6, and B atoms along both the *endo* and *exo* channels were observed.

The atoms whose population showed larger changes along the reaction coordinate and different behavior related to the nature of the substituents on the boron atom were C_1 and B. The variation of the population of C_2, C_3, and C_6 was smaller and presented almost similar profiles for the reactions with the dienophiles under study (see the Supporting Information). Figure 7 displays the variations of the electron populations of the C_1 and B atoms along the course of the reactions with **1**, **3**, **5**, **10**, **11**, and **12** corresponding to the lowest-energy pathways. C_1 had the highest electron population among the analyzed carbon atoms, that is, presented the largest negative net charge. The atomic populations of C_1 were in the range of 6.58–6.77 au for all reactions except for the one with **12**. The changes

dx.doi.org/10.1021/jp504972r | J. Phys. Chem. A 2014, 118, 5559−5570

were more pronounced for the reactions with **1**, **3**, and **5** than for those with **10** and **11**. The atomic populations increased from the early steps of the reactions up to a maximum after the TSs, and then, it decreased toward the product formation. For the reaction with **12**, the electron population of C_1 remained almost constant until the TS; then it decreased slightly, reaching a minimum, and finally, it increased slightly. The electron population of the B atom changed considerably along the reaction coordinates for the reactions with **1**, **3**, and **5**, while for the reactions with **10**, **11**, and **12**, the changes were less significant. These results suggest that larger variations of the electron population are related to lower activation free energies. This might be mainly due to the fact that there is more redistribution of the charge density affecting the net charges of the atom, in particular, the C_1 and B atoms along the course of the reaction.

CONCLUSIONS

In this study, the effect of the nature of the boron moiety on the reactivity and the selectivity of a series of vinylboron compounds in the DA reaction with cyclopentadiene has been investigated using DFT methods and the QTAIM approach. The calculated reactivity of the dienophiles decreases in the order vinylborane (**1**) > dihalovinylboranes (**2**−**4**) > dialkylvinylboranes (**5**−**7**) ≈ vinyl boronic acid (**8**) > vinylboronates (**9** and **10**) > tetracoordinated organoboron dienophiles (**11** and **12**). These results are in agreement with the experimental data available.

All of the TSs show a topological pattern typical of [4 + 2] TSs because the bcps corresponding to the C_1-C_6 and C_2-C_3 forming bonds and a ring critical point associated with the six-membered ring were found. The bond distances together with the values of ρ_b and $\nabla^2\rho_b$ indicated that the C_2-C_3 forming bond is more advanced than the C_1-C_6 forming bond in TSs of **1**−**11**, while for the TSs of **12**, the C_1-C_6 bond has a slightly greater degree of formation.

Calculations correctly predicted that the DA reactions of **1**−**5** and **7** are slightly *endo*-selective, which was mainly attributed to the stronger C_6-B secondary orbital interaction in the *endo* TSs evaluated by the $C_6|B$ DIs. The *exo* selectivities calculated for the DA reaction of boronates **8**−**11** were rationalized in terms of the hydrogen bond between the oxygen atom of the boronate moieties and one of the acidic hydrogens of the methylene of cyclopentadiene in the *exo* TSs. This interaction reduces the ability of the oxygen lone pairs to donate electron density into the vacant boron orbital. Interestingly, the two hydrogen bonds and the existence of a cooperative effect between them in the *exo* TS of the DA reaction of vinyltrifluoroborate (**12**) determine the almost exclusive *exo* selectivity (*endo*/*exo* 3:97) predicted for this DA reaction.

The topological properties ρ_r and L_r of the Laplacian of the electron density evaluated at the (3, +1) critical points on the isolated dienophiles indicated that C_2 is more susceptible to nucleophilic attack than C_1 for dienophiles **1**−**11**, while for **12**, this is inverted, in accordance with the geometrical and topological data of the TSs. Interestingly, for dienophiles **1**−**11**, a good linear correlation between ρ_r and L_r at the (3, +1) critical points on C_2 and the activation free energy ($\Delta G^{\#}$) were obtained. We propose that the Lapacian of the charge density analysis is a simple and valuable tool to identify the reactive site and to properly estimate the reactivity of neutral boron-activated dienophiles, which only needs the information about the reagent molecules in their ground state. Also, it has the advantage of being based on a real physical property of the system. Further studies on this subject are needed to extend the scope of this approach.

The analysis of ρ_b and $\nabla^2\rho_b$ at the bcp corresponding to the forming bonds and DI of $C_6|B$ along the reaction coordinates demonstrated that although the C_6-B interaction is weak, the boron atom and the nature of the substituents affect the distribution of the surrounding electron charge density and the mode of addition.

The ellipticity evaluated at the C_1-C_6 bcp along the reaction coordinates shows different profiles depending on the structure of the dienophiles and the mode of addition (*exo* and *endo*). In addition, the variation of this topological parameter along with those for the atomic population of C_1 and B demonstrates that the electron distribution is strongly related to the stabilization of the system and therefore to the selectivity of the reaction.

The results obtained herein allowed us to gain a deeper knowledge of the studied DA reactions and encourage further experimental and theoretical studies of new related reactions in our laboratories.

ASSOCIATED CONTENT

Supporting Information

Molecular graphs, the relationship between ΔR and $\Delta\rho_b$, the relationship between the free energy ($\Delta G^{\#}$) and charge transfer (CT), topological properties, and the electron population along the IRC coordinates. This material is available free of charge via the Internet at http://pubs.acs.org.

AUTHOR INFORMATION

Corresponding Authors

*E-mail: vallejos.marga@gmail.com. Phone/Fax: +54-379-4457996, int. 104 (M.M.V.).

*E-mail: pellegrinet@iquir-conicet.gov.ar. Phone/Fax: +54-341-4370477 (S.C.P.).

Present Address

†M.M.V.: Departamento de Química, Facultad de Ciencias Exactas y Naturales y Agrimensura, Universidad Nacional del Nordeste, Avda. Libertad 5460, (3400) Corrientes, Argentina.

Notes

The authors declare no competing financial interest.

ACKNOWLEDGMENTS

We thank CONICET, ANPCyT and UNR. M. M. V. thanks UNNE, and SECYT-UNNE. N. G. thanks Fundación Josefina Prats.

REFERENCES

(1) Dell, C. P. Cycloadditions in Synthesis. *J. Chem. Soc., Perkin Trans. 1* **1998**, 3873−3905.

(2) Nicolaou, K. C.; Snyder, S. A.; Montagnon, T.; Vassilikogiannakis, G. The Diels−Alder Reaction in Total Synthesis. *Angew. Chem., Int. Ed.* **2002**, *41*, 1668−1698.

(3) Sauer, J.; Sustmann, R. Mechanistic Aspects of Diels−Alder Reactions: A Critical Survey. *Angew. Chem., Int. Ed. Engl.* **1980**, *19*, 779−807.

(4) Hilt, G.; Bolze, P. Boron-Substituted Building Blocks in Diels−Alder and Other Cycloaddition Reactions. *Synthesis* **2005**, 2091−2115.

(5) Hall, D. G. *Boronic Acids*; Wiley-VCH: Weinheim, Germany, 2005.

(6) Singleton, D. A.; Martinez, J. P.; Ndip, G. M. In Situ Formation of Vinylboranes for Use in Diels−Alder Reactions. An Easy One-Pot

Diels–Alder Synthesis of Cyclohexenols. *J. Org. Chem.* **1992**, *57*, 5768–5771.
(7) Zaidlewicz, M.; Binkul, J. R.; Sokół, W. Syntheses with Organoboranes. IX. Vinyl- and 1-Alkenyldichloroboranes as Ethylene and 1-Alkene Equivalents for the Diels–Alder Reaction. *J. Organomet. Chem.* **1999**, *580*, 354–362.
(8) The reaction of dicholorovinylborane with cyclopentadiene was described earlier by Vaultier and co-workers to give a 50:50 mixture of the *endo* and *exo* boronic esters in 60% yield after treatment with pinacol; see: Noiret, N.; Youssofi, A.; Carboni, B.; Vaultier, M. *Chem. Soc., Chem. Commun.* **1992**, 1105–1107.
(9) Matteson, D. S.; Waldbillig, J. O. Norborneneboronates. *J. Org. Chem.* **1963**, *28*, 366–369.
(10) Matteson, D. S.; Talbot, M. L. Bicyclo[2.2.2]Octeneboronic Acids and Their Reaction with Mercuric Chloride. *J. Am. Chem. Soc.* **1967**, *89*, 1123–1126.
(11) Vallejos, M. M.; Grimblat, N.; Pellegrinet, S. C. Diels-Alder Reactions of Pinacol Alkenylboronates: An Experimental and Theoretical Study. *Org. Biomol. Chem.* Manuscript submitted for publication.
(12) Singleton, D. A. A [4 + 3] Transition State for a [4 + 2] Cycloaddition. A New Secondary Orbital Interaction in Diels–Alder Reactions. *J. Am. Chem. Soc.* **1992**, *114*, 6563–6564.
(13) Pellegrinet, S. C.; Silva, M. A.; Goodman, J. M. Theoretical Evaluation of the Origin of the Regio- and Stereoselectivity in the Diels–Alder Reactions of Dialkylvinylboranes: Studies on the Reactions of Vinylborane, Dimethylvinylborane, and Vinyl-9-BBN with *trans*-Piperylene and Isoprene. *J. Am. Chem. Soc.* **2001**, *123*, 8832–8837.
(14) Silva, M. A.; Pellegrinet, S. C.; Goodman, J. M. Diels–Alder Reactions of Vinylboranes: A Computational Study on the Boron Substituent Effects. *Arkivoc* **2003**, 556–565.
(15) Grimblat, N.; Pellegrinet, S. C. Theoretical Investigation of the Diels–Alder Reactions of Unsaturated Boronates. *Org. Biomol. Chem.* **2013**, *11*, 3733–3741.
(16) Bader, R. F. W. *Atoms in Molecules. A Quantum Theory*; Oxford Science Publications, Clarendon Press: London, 1990.
(17) Matta, C. F.; Boyd, R. J. *The Quantum Theory of Atoms in Molecules: From Solid State to DNA and Drug Design*; Wiley-VCH: Weinheim, Germany, 2007.
(18) Bader, R. F. W. A Quantum Theory of Molecular Structure and Its Applications. *Chem. Rev.* **1991**, *91*, 893–928.
(19) Alikhani, M. E. On the Chemical Bonding Features in Boron Containing Compounds: A Combined QTAIM/ELF Topological Analysis. *Phys. Chem. Chem. Phys.* **2013**, *15*, 12602–12609.
(20) Werstiuk, N. H.; Sokol, W. QTAIM–DI–VISAB Computational Study on the Diels–Alder Reaction of Cyclopentadiene — On the Nature of the So-Called Secondary Orbital Interactions. *Can. J. Chem.* **2008**, *86*, 737–744.
(21) Brown, E. C.; Bader, R. F. W.; Werstiuk, N. H. Qtaim Study on the Degenerate Cope Rearrangements of 1,5-Hexadiene and Semibullvalene. *J. Phys. Chem. A* **2009**, *113*, 3254–3265.
(22) Rode, J. E.; Dobrowolski, J. C. Variation of Bcp Ellipticities in the Course of the Pericyclic and Pseudopericyclic [2 + 2] Cycloaddition Reactions of Cumulenes. *Chem. Phys. Lett.* **2007**, *449*, 240–245.
(23) Rode, J. E.; Dobrowolski, J. C. Reaction Paths of the [2 + 2] Cycloaddition of XCY Molecules (X, Y = S or O or CH_2). Ab Initio Study. *J. Phys. Chem. A* **2006**, *110*, 207–218.
(24) Rode, J. E.; Dobrowolski, J. C. An Ab Initio Study on the Allene–Isocyanic Acid and Ketene–Vinylimine [2 + 2] Cycloaddition Reaction Paths. *J. Phys. Chem. A* **2006**, *110*, 3723–3737.
(25) López, C. S.; Faza, O. N.; Cossío, F. P.; York, D. M.; de Lera, A. R. Ellipticity: A Convenient Tool to Characterize Electrocyclic Reactions. *Chem.—Eur. J.* **2005**, *11*, 1734–1738.
(26) López, C. S.; Lera, Á. R. d. Bond Ellipticity as a Measure of Electron Delocalization in Structure and Reactivity. *Curr. Org. Chem.* **2011**, *15*, 3576–3593.
(27) Calvo-Losada, S.; Quirante Sánchez, J. J. Pericyclic versus Pseudopericyclic Reactions. What the Laplacian of the Charge Density, $\nabla^2\rho_{(r)}$, Has to Say About It? The Case of Cycloaddition Reactions. *J. Phys. Chem. A* **2008**, *112*, 8164–8178.
(28) Wagner, G.; Danks, T. N.; Vullo, V. Quantum-Chemical Study of the Lewis Acid Influence on the Cycloaddition of Benzonitrile Oxide to Acetonitrile, Propyne and Propene. *Tetrahedron* **2007**, *63*, 5251–5260.
(29) Zalazar, M. F.; Peruchena, N. M. Topological Analysis of the Electronic Charge Density in the Ethene Protonation Reaction Catalyzed by Acidic Zeolite. *J. Phys. Chem. A* **2007**, *111*, 7848–7859.
(30) Patil, M. P.; Sunoj, R. B. Density Functional Theory and Atoms-in-Molecule Study on the Role of Two-Electron Stabilizing Interactions in Retro Diels–Alder Reaction of Cycloadducts Derived from Substituted Cyclopentadiene and P-Benzoquinone. *Org. Biomol. Chem.* **2006**, *4*, 3923–3930.
(31) Vallejos, M. M.; Peruchena, N. M.; Pellegrinet, S. C. [4 + 3] and [4 + 2] Mechanisms of the Diels–Alder Reactions of Vinylboranes: An Analysis of the Electron Charge Density Distribution. *Org. Biomol. Chem.* **2013**, *11*, 7953–7965.
(32) Uno, B. E.; Gillis, E. P.; Burke, M. D. Vinyl MIDA Boronate: A Readily Accessible and Highly Versatile Building Block for Small Molecule Synthesis. *Tetrahedron* **2009**, *65*, 3130–3138.
(33) Gillis, E. P.; Burke, M. D. Multistep Synthesis of Complex Boronic Acids from Simple MIDA Boronates. *J. Am. Chem. Soc.* **2008**, *130*, 14084–14085.
(34) Knapp, D. M.; Gillis, E. P.; Burke, M. D. A General Solution for Unstable Boronic Acids: Slow-Release Cross-Coupling from Air-Stable MIDA Boronates. *J. Am. Chem. Soc.* **2009**, *131*, 6961–6963.
(35) Gillis, E. P.; Burke, M. D. A Simple and Modular Strategy for Small Molecule Synthesis: Iterative Suzuki–Miyaura Coupling of B-Protected Haloboronic Acid Building Blocks. *J. Am. Chem. Soc.* **2007**, *129*, 6716–6717.
(36) Molander, G. A.; Ellis, N. Organotrifluoroborates: Protected Boronic Acids That Expand the Versatility of the Suzuki Coupling Reaction. *Acc. Chem. Res.* **2007**, *40*, 275–286.
(37) Hall, D. G. *Boronic Acids: Preparation and Applications in Organic Synthesis, Medicine and Materials*, 2nd completely rev. ed.; Wiley-VCH: Weinheim, Germany, 2011.
(38) Becke, A. D. Density-Functional Thermochemistry. III. The Role of Exact Exchange. *J. Chem. Phys.* **1993**, *98*, 5648–5652.
(39) Parr, R. G.; Yang, W. *Density Fuctional Theory of Atoms and Molecules*; Oxford University Press: New York, 1989.
(40) Frisch, M. J.; Trucks, G. W.; Schlegel, H. B.; Scuseria, G. E.; Robb, M. A.; Cheeseman, J. R.; Scalmani, G.; Barone, V.; Mennucci, B.; Petersson, G. A.; Nakatsuji, H.; et al. *Gaussian 09*, revision D.01; Gaussian, Inc.: Wallingford, CT, 2009.
(41) Cremer, D.; Kraka, E. Chemical Bonds without Bonding Electron Density — Does the Difference Electron-Density Analysis Suffice for a Description of the Chemical Bond? *Angew. Chem., Int. Ed. Engl.* **1984**, *23*, 627–628.
(42) Merino, G.; Vela, A.; Heine, T. Description of Electron Delocalization Via the Analysis of Molecular Fields. *Chem. Rev.* **2005**, *105*, 3812–3841.
(43) Keith, T. A. *Aimall*, version 11.12.19; TK Gristmill Software: Overland Park, KS, 2011.
(44) Biegler-König, F. Calculation of Atomic Integration Data. *J. Comput. Chem.* **2000**, *21*, 1040–1048.
(45) Singleton, D. A.; Martinez, J. P. High Reactivity, Regioselectivity, and Endo-Stereoselectivity of Vinyl Boranes in Diels–Alder Reactions. *J. Am. Chem. Soc.* **1990**, *112*, 7423–7424.
(46) Singleton, D. A.; Martinez, J. P.; Watson, J. V.; Ndip, G. M. Tuning of Vinylborane Dienophilicity. Optimization of Reactivity, Regioselectivity, Endo-Stereoselectivity, and Reagent Stability. *Tetrahedron* **1992**, *48*, 5831–5838.
(47) Espinosa, E.; Alkorta, I.; Elguero, J.; Molins, E. From Weak to Strong Interactions: A Comprehensive Analysis of the Topological and Energetic Properties of the Electron Density Distribution Involving X–H···F–Y Systems. *J. Chem. Phys.* **2002**, *117*, 5529–5542.

(48) Jeffrey, G. A. *An Introduction to Hydrogen Bonding*; Oxford University Press: Oxford, U.K., 1997.
(49) Koch, U.; Popelier, P. L. A. Characterization of C−H···O Hydrogen Bonds on the Basis of the Charge Density. *J. Phys. Chem.* **1995**, *99*, 9747−9754.
(50) Rozas, I.; Alkorta, I.; Elguero, J. Behavior of Ylides Containing N, O, and C Atoms as Hydrogen Bond Acceptors. *J. Am. Chem. Soc.* **2000**, *122*, 11154−11161.
(51) Reed, A. E.; Curtiss, L. A.; Weinhold, F. Intermolecular Interactions from a Natural Bond Orbital, Donor−Acceptor Viewpoint. *Chem. Rev.* **1988**, *88*, 899−926.
(52) Domingo, L. R.; Saez, J. A. Understanding the Mechanism of Polar Diels−Alder Reactions. *Org. Biomol. Chem.* **2009**, *7*, 3576−3583.
(53) Domingo, L. R.; Arnó, M.; Andrés, J. Influence of Reactant Polarity on the Course of the Inverse-Electron-Demand Diels−Alder Reaction. A DFT Study of Regio- and Stereoselectivity, Presence of Lewis Acid Catalyst, and Inclusion of Solvent Effects in the Reaction between Nitroethene and Substituted Ethenes. *J. Org. Chem.* **1999**, *64*, 5867−5875.
(54) Sarotti, A. M. Unraveling Polar Diels−Alder Reactions with Conceptual DFT Analysis and the Distortion/Interaction Model. *Org. Biomol. Chem.* **2014**, *12*, 187−199.
(55) Popelier, P. L. A. On the Full Topology of the Laplacian of the Electron Density. *Coor. Chem. Rev.* **2000**, *197*, 169−189.
(56) Bader, R. F. W.; Chang, C. Properties of Atoms in Molecules: Electrophilic Aromatic Substitution. *J. Phys. Chem.* **1989**, *93*, 2946−2956.
(57) Tafipolsky, M.; Scherer, W.; Öfele, K.; Artus, G.; Pedersen, B.; Herrmann, W. A.; McGrady, G. S. Electron Delocalization in Acyclic and N-Heterocyclic Carbenes and Their Complexes: A Combined Experimental and Theoretical Charge-Density Study. *J. Am. Chem. Soc.* **2002**, *124*, 5865−5880.
(58) Carroll, M. T.; Cheeseman, J. R.; Osman, R.; Weinstein, H. Nucleophilic Addition to Activated Double Bonds: Predictions of Reactivity from the Laplacian of the Charge Density. *J. Phys. Chem.* **1989**, *93*, 5120−5123.
(59) Popelier, P. L. A. *Atoms in Molecules. An Introduction*; Pearson Education: Harlow, U.K., 2000.
(60) The global electrophilicity index (ω) for the reactants was calculated as $\omega = \mu^2/2\eta$ (eV), where μ is the electronic chemical potential and η the chemical hardness. Both quantities were estimated on the basis of the one-electron energies from the HOMO and LUMO (ε_{HOMO} and ε_{LUMO}) as $\mu \approx (\varepsilon_{HOMO} + \varepsilon_{LUMO})/2$ and $\eta \approx (\varepsilon_{LUMO} - \varepsilon_{HOMO})$.
(61) Bader, R. F. W.; Slee, T. S.; Cremer, D.; Kraka, E. Description of Conjugation and Hyperconjugation in Terms of Electron Distributions. *J. Am. Chem. Soc.* **1983**, *105*, 5061−5068.
(62) Matta, C. F.; Arabi, A. A.; Keith, T. A. Atomic Partitioning of the Dissociation Energy of the P−O(H) Bond in Hydrogen Phosphate Anion (HPO_4^{2-}): Disentangling the Effect of Mg^{2+}. *J. Phys. Chem. A* **2007**, *111*, 8864−8872.
(63) Arabi, A. A.; Matta, C. F. Where Is Electronic Energy Stored in Adenosine Triphosphate? *J. Phys. Chem. A* **2009**, *113*, 3360−3368.
(64) Vallejos, M. M.; Angelina, E. L.; Peruchena, N. M. Bifunctional Hydrogen Bonds in Monohydrated Cycloether Complexes. *J. Phys. Chem. A* **2010**, *114*, 2855−2863.
(65) Vallejos, M. M.; Peruchena, N. M. Preferential Formation of the Different Hydrogen Bonds and Their Effects in Tetrahydrofuran and Tetrahydropyran Microhydrated Complexes. *J. Phys. Chem. A* **2012**, *116*, 4199−4210.